Analysis and Synthesis of Transmitarray Antennas for Near-Field Shaping

Sergio M. Feito[1,2], Francesco Foglia Manzillo[2], Antonio Clemente[2], Manuel Arrebola[1]

[1] Group of Signal Theory and Communications, Universidad de Oviedo, Gijón, Spain, {menendezfsergio, arrebola}@uniovi.es

[2] CEA - Leti, Univ. Grenoble-Alpes, F-38000 Grenoble, France, {francesco.fogliamanzillo, antonio.clemente}@cea.fr

***Abstract*- In this study, we propose a method based on the Intersection Approach to create near-field patterns for transmitarray antennas. Initially, we describe a model for calculating the amplitude and phase of the electric field in the near-field region and validate by comparison with full-wave simulations. We then present the proposed phase-only synthesis algorithm. Utilizing fast Fourier transforms, this algorithm iteratively searches for a viable aperture phase profile fulfilling the near-field pattern constraints. We apply this method to create a transmitarray that produces a near-field shaped pattern on a plane parallel to the aperture. Lastly, we discuss the effects of uniform phase quantization on the near-field pattern shape and peak amplitude.**

I. Introduction

The analysis and synthesis of near-field antennas have generated a growing interest for various applications, such as wireless power transfer [1], medical scanners and hyperthermia treatments [2], and next-generation smart access points [3]. For these applications, it is essential to shape the radiated near-field (NF) in specific planes or volumes [4].

Spatially fed arrays (SFA), including transmitarray (TA), metalens, and reflectarray (RA) antennas, offer a practical and energy-efficient approach to shaping the near field in the Fresnel region. TAs consist of radiating elements, known as unit cells (UCs), which introduce a phase shift on an incident electromagnetic field before re-radiating it. By designing the UCs and their distribution on the TA aperture, the radiated electromagnetic field can be tailored with minimal losses, unlike phased array architectures.

Numerous methods for synthesizing spatially fed arrays (SFAs) have been proposed in the literature, employing different mathematical approaches, such as the Intersection Approach (IA) [5] or convex optimization [6]. However, most of these works focus on far-field (FF) synthesis, with only a few procedures presented for near-field shaping [7]-[9]. For example, in [8], the near field (NF) is obtained as the sum of the farfields emitted by each UC, which increases computation time with respect rather to methods based on a single Fourier transform of the aperture field. Following a similar approach, the synthesis of non-diffractive beams is demonstrated in [9]. Furthermore, most NF-shaped transmitarrays (TAs) found in the literature are essentially 2.5-D dielectric discrete lenses [8], [9], where the height of each UC is adjusted to approximate the optimal phase shift distribution. However, this method is unsuited for realizing TAs using planar technologies. In these planar designs, only a discrete set of different UCs, often leading to a coarse phase quantization [10], [11], is usually employed to improve the common transmission bandwidth and simplify the manufacturing process.

In this work, we present a computationally efficient synthesis tool, based on the IA, for arbitrarily shaping the NF pattern of a TA, on a plane parallel to its aperture. Additionally, we investigate the effect of an N-bit phase quantization of the optimized phase profile on the amplitude of the near-field. The numerical results validate the analysis model and demonstrate the effectiveness of the proposed synthesis method.

II. Transmitarray Optics and Analysis

A. Modeling the transmitarray

Fig. 1 depicts the structure of the TA under analysis. The TA consists of a focal source and an $M\times N$ planar array of identical UCs, located at a distance F from the feed. The lens edges have lengths D_x and D_y, while the center-to-center distance between adjacent UCs are d_x and d_y along the x- and y-axis, respectively. The UCs modify the impinging electric field on the receiving side, which is then transformed into the tangent electric field $\vec{E}_{AP}$ on the transmitting side of the TA. The UCs are generally designed to introduce minimal losses and mainly alter the incident field by introducing a phase shift and/or polarization manipulation. The distribution of the different UCs in the TA and, consequently, the spatial phase profile of $\vec{E}_{AP}$ must be optimized to achieve the desired NF pattern. Assuming a uniform field distribution within each UC, $\vec{E}_{AP}$ over the mn-th cell can be expressed as:

$$\vec{E}_{AP}(x_m, y_n) = \boldsymbol{T}^{mn} \cdot \vec{E}_{inc}(x_m, y_n), \qquad (1)$$

where the transmission coefficient matrix T^{mn} characterizes the transmission properties of the mn-th cell, and $\vec{E}_{inc}^{mn}(x_m, y_n)$ is the incident field received from the feed at the center of the cell, with coordinates (x_m, y_n).

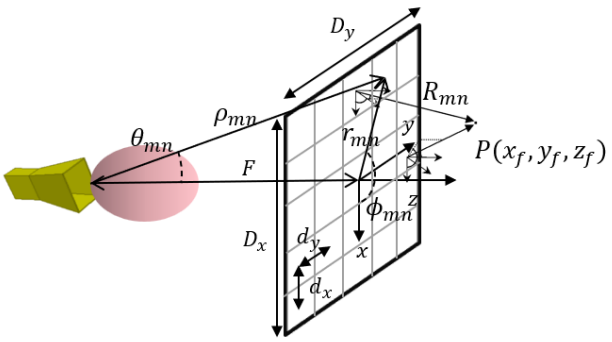

Fig. 1. Sketch of the transmitarray geometry.

If one neglects the spillover radiation, the i-component E_{NF}^{i} of the near field emitted in free space by the TA, on a plane

parallel to the radiating aperture at a distance z_0 from it, can be found using the fast Fourier transform (FFT):

$$E^i_{NF}(x,y,z_0) = \frac{1}{4\pi^2}\mathcal{F}^{-1}\{g_p\mathcal{F}\{E_{AP}(x,y)\}\} \quad (2)$$

where $\mathcal{F}$ and $\mathcal{F}^{-1}$ are the operators for direct and inverse Fourier transforms, respectively. It is assumed that the aperture field has only one non-zero component (E_{AP}). The factor $g_p = e^{-jk_z z_0}$ [12] represents a spatial translation by z_0 along the z-axis, where k_z is the z-component of the wave vector, given by:

$$k_z = \begin{cases} \sqrt{k_0^2 - k_x^2 - k_y^2}\,, k_0^2 \geq k_x^2 + k_y^2 \\ -j\sqrt{-k_0^2 + k_x^2 + k_y^2}\,, k_0^2 < k_x^2 + k_y^2 \end{cases}, \quad (3)$$

being k_0 the free-space propagation constant, k_x and k_y the spectral frequencies extending over the entire spectrum [14].

B. Validation of the model

To verify the accuracy of the model discussed in Section II-A, a near-field focusing TA was designed using the set of 16 UCs presented in [13]. The numerical predictions obtained from the model were compared with the results of a full-wave simulation of the entire antenna. The NF-focusing TA consists of 24×24 square elements, with a periodicity $d_x = d_y = 0.35\,\lambda$, where λ is the free-space wavelength at the operating frequency (140 GHz). The TA is fed by a 10-dBi pyramidal horn that is aligned with the centre of the array, at a distance $F = 0.8D_x$ (see Fig. 1). The phase profile of the TA is determined using the conjugate-phase approach [3], to focus the field at the point $P \equiv (0, 0, 0.1D_{ff})$, where $D_{ff} \cong 141\lambda$ is the far-field distance at 140 GHz. Specifically, the phase shift introduced by the mn-th UC whose center is at a distance R_{mn} from P is set to:

$$\chi_{mn} = \frac{2\pi}{\lambda} R_{mn} - \angle\vec{E}_{inc}(x_m, y_n) \quad (4)$$

This phase profile maximizes the amplitude of the near-field in P, except for a small shift caused by the field spreading factor. However, this conjugate-phase design does not provide control on the shape of the near-field pattern.

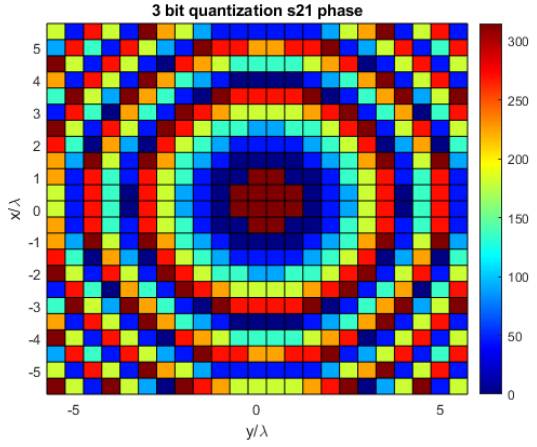

Fig. 2. The spatial profile of the UC phase shifts, in degrees, on the 24×24 TA designed using the conjugate-phase approach, to focus the y-component of the electric field in the point $P \equiv (0, 0, 14.1\lambda)$ is shown.

The optimal phase shift in (4) has been approximated using the simulated values of the 16 UCs, which achieve an almost uniform 4-bit quantization of the 2π range. The resulting spatial profile of the UC phase shift is shown in Fig. 2. The UCs are designed with two wire grid polarizers on the outer layers, which rotate the polarization of the incident field by 90° and result in an almost purely y-polarized aperture field. The near field is computed on the focusing plane ($z = 14.1\lambda$) using the simulated complex transmission coefficients t_{yx} of the 16 UCs, assuming normal incidence and local periodicity, and the simulated far-field radiation pattern of the horn to determine the incident field on the array. The x-cut of the near-field pattern (y-component of the electric field) is shown in Fig. 3, and the predictions of the proposed model are in excellent agreement with the full-wave simulation of the TA. Notably, the model accurately computes the amplitude of the near-field. The difference between the computed and simulated peak values is only 0.7 dB. This is noteworthy as most prior research on near-field focusing and shaping TAs compare only normalized patterns [7]-[9].

III. Intersection Approach Based Synthesis Procedure

A. Description of the algorithm

The synthesis method employed in this study relies on the Intersection Approach. Two masks, T_{upper} and T_{lower}, are imposed as upper and lower limits for the near-field amplitude.

The iterative algorithm involves the application of two operators: the forward propagation operator $\mathcal{P}$, described by the right-hand side of (2), and the backward propagation operator $\mathcal{B}$, which can be expressed as follows:

$$E_{AP}(x,y) = \frac{1}{4\pi^2}\mathcal{F}^{-1}\left\{g_b\mathcal{F}\left\{E^i_{NF}(x,y,z_0)\right\}\right\}, \quad (5)$$

Where $g_b = e^{jk_z hz_0}$The expression for k_z is similar to that in (3). However, when the second condition ($k_o^2 < k_x^2 + k_y^2$) is met, the positive imaginary root is retained.

As illustrated in the diagram depicted in Fig. 4, the procedure starts with a known input tangential field distribution over the aperture and computes the near field using the forward propagator ($\mathcal{P}$). Each UC of the TA is treated as a rectangular aperture antenna with a uniform field distribution for this computation [14]. However, the near field (E^i_{NF}) associated to this aperture field usually fails to meet the imposed constraints. Hence, a new near field $\tilde{E}_{NF}$ is constructed by modifying its amplitude and keeping its phase unchanged. This new near-field satisfies the amplitude mask constraints. Formally, the correction of the NF amplitude can be expressed as:

$$|\tilde{E}^i_{NF}| = \begin{cases} T_{upper}\,; & if\ \ E_{NF} \geq T_{upper} \\ T_{lower}\,; & if\ \ E_{NF} \leq T_{lower} \\ |E^i_{NF}|; & otherwise \end{cases} \quad (6)$$

After obtaining the modified near field $\tilde{E}^i_{NF}$, the backward propagation ($\mathcal{B}$) is used to find the field distribution $\tilde{E}_{AP}$ that generates $\tilde{E}^i_{NF}$. However, since the amplitude of the field on the TA aperture is dependent on the incident field, it cannot be ensured $\tilde{E}^i_{AP}$ is a feasible tangential field. Only the phase of $\tilde{E}_{AP}$ can be adjusted by distributing the UCs in the TA. Therefore, the following feasible aperture field (E_{AP}) is prescribed, after the backward propagation, to be used in the next iteration of the algorithm:

$$E_{AP} = \begin{cases} |E_{inc}|e^{j\angle\tilde{E}_{ap}}\,; & |x| \leq \frac{D_x}{2}\,, |y| \leq \frac{D_y}{2}\,, \\ 0\,; & otherwise \end{cases} \quad (7)$$

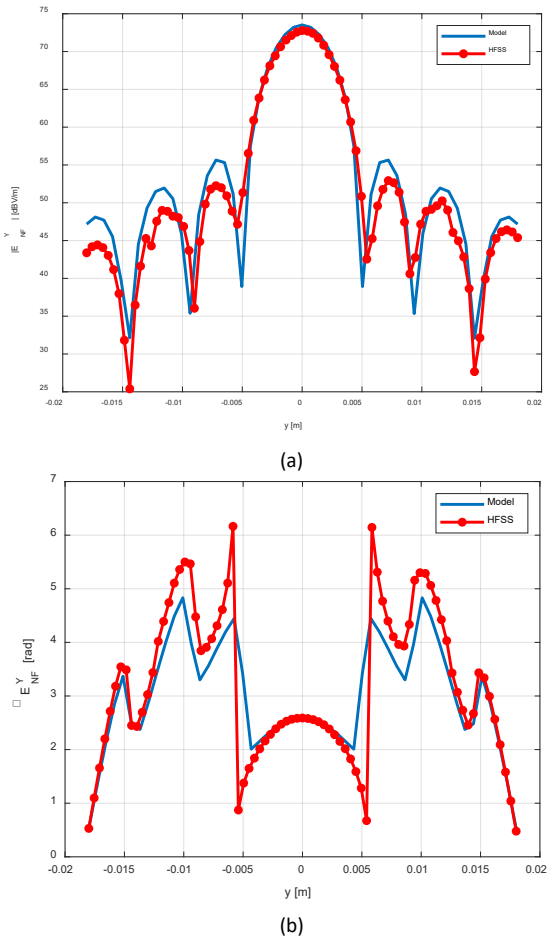

Fig. 3. Comparison of the results of the model and of full-wave simulations for the 24×24 TA designed with a conjugate-phase approach. (a) Amplitude and (b) Phase of the y-component of the radiated field along the y-axis, at $z = 0.1\ D_{ff}$.

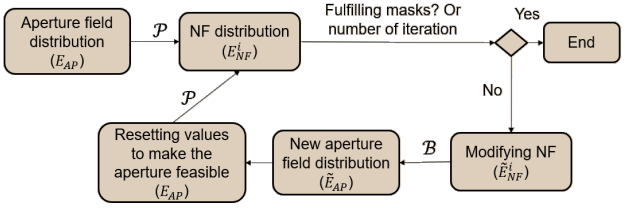

Fig. 4. Flowchart of the classical Intersection Approach used for the synthesis TAs.

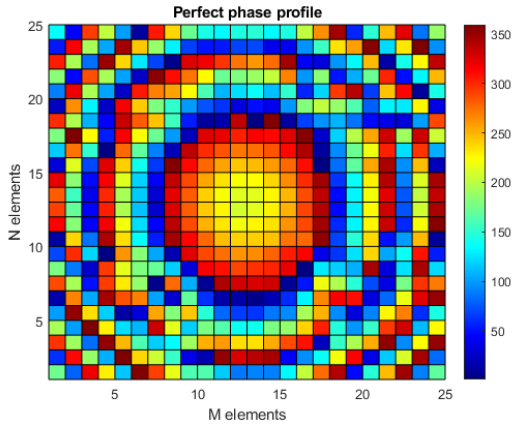

Fig. 5. Synthesised phase shift distribution (in degrees) introduced by the unit cells of the 24×24 near-field shaped TA assuming perfectly transmitting UCs.

Iterating the presented procedure, a solution that satisfies both the physical constraints on the aperture field and the near-field pattern constraints may be found.

B. Synthesis of a shaped-beam near-field pattern

This subsection describes a numerical example of TA synthesis for NF shaping. The desired NF has a fan-beam pattern on a plane located at $z = 22\lambda$, with a -3-dB spot measuring 3λ ×6λ. Additionally, a maximum amplitude ripple of 0.6 dB is required in the y-cut flat-top region. To achieve this, a 24×24 TA fed by a 10-dBi horn is considered. Each UC measures $\lambda/2 \times \lambda/2$, where λ represents the wavelength at the optimization frequency. The feed is positioned at a distance $F = 0.1$ m from the lens. The incident field on the TA is calculated using its simulated far-field pattern.

Using the aperture-field distribution that compensates for the phase of the incident field and produces a far-field boresight pencil beam as the starting point, the synthesis procedure successfully converged. The NF pattern fulfills the required masks in all points, despite the significant difference between the desired and initial NF patterns. The convergence was achieved after about 1000 iterations in 340 seconds. The synthesized phase profile introduced by the lens on the incident field is depicted in Fig. 5.It is exhibiting a consistent symmetry with respect to the aperture center, as expected physically given the pattern constraints. The enforced mask and the y- and x-cut of the near-field pattern on the target plane are reported in Fig. 6 and Fig. 7, respectively.

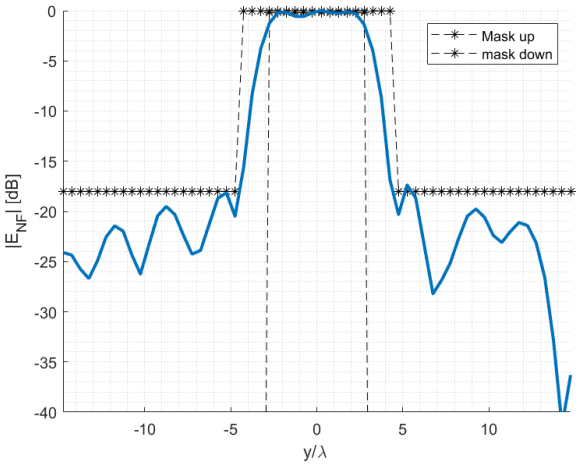

Fig. 6. NF pattern (x=0 cut) of the synthesized 24×24 TA, at a distance of 22λ from the TA radiating aperture, using the UC phase profile of Fig. 5

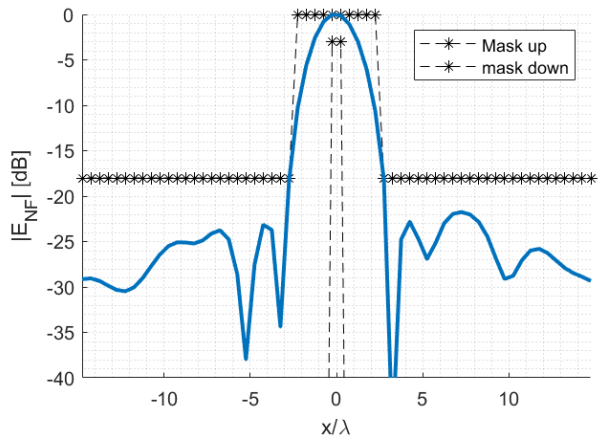

Fig. 7. NF pattern (y=0 cut) of the synthesized 24×24 TA, at a distance of 22λ from the TA radiating aperture, using the UC phase profile of Fig. 5.

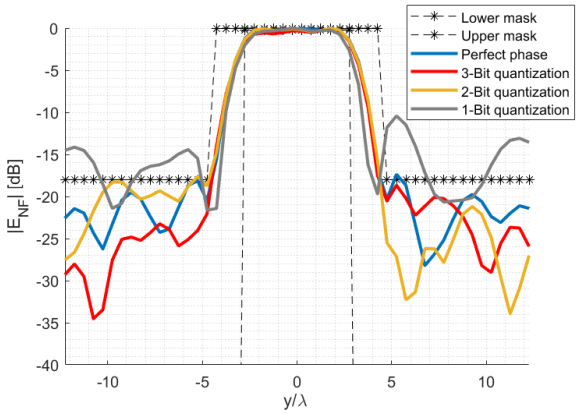

Fig. 8. NF pattern (x=0 cut) of the 24×24 synthesized TA, at 22λ from the aperture, for different n-bit quantization of the optimal phase distribution of Fig. 5.

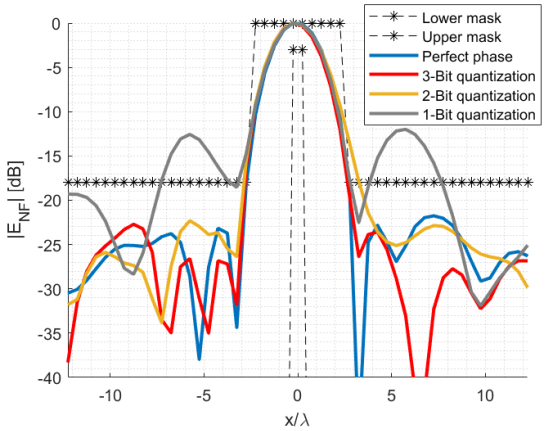

Fig. 9. NF pattern (y=0 cut) of the 24×24 TA, at a distance of 22λ from the aperture, for different n-bit quantization of the optimal phase distribution of Fig. 5.

C. *Impact of phase quantization*

In Section III-B, we assumed that the UCs could introduce any phase shift value, which would allow them to perfectly realize the optimal phase profile. However, in practical designs, especially in electronically reconfigurable TAs, only a limited number of different UCs can be used, which provides a discrete set of phase shifts. Designing a large number of UCs can be time-consuming, technologically challenging, and limit the common operating bandwidth. Therefore, it is crucial to evaluate the impact of phase quantization on the near field after the synthesis. Although the results will depend on the mask and the plane where it is enforced, the synthesized TA discussed in Section III-B is a relevant benchmark example because its phase profile is relatively fast-varying due to the challenging mask constraints. Thus, we approximated the synthesized phase profile using three sets of 2^n UCs, where n =1, 2, 3. The phases of the transmission coefficients of each set are uniformly distributed in the [0, 2π) range.

Fig. 8 and Fig. 9 illustrate the near-field patterns achieved for various values of n. The x-cut is found to be more affected by coarse phase quantization compared to the y-cut. Nonetheless, even a 1-bit quantization noticeably increases the SLL outside the flat-top region. Further investigation shows that a 3-bit quantization or higher can effectively satisfy the mask constraints in most of the points, while minimizing NF pattern distortion and peak amplitude loss.

IV. Conclusion

This study introduces a novel model for the analysis and synthesis of the near field radiated by transmitarray antennas. The analysis framework has been validated through comparison with full-wave simulations. Unlike previous research, this model accurately predicts both the normalized near-field pattern and the electric field amplitude. A phase-only synthesis procedure has been proposed that allows one to shape a component of the electric field on planes parallel to the aperture. The proposed algorithm, resorts to the Intersection Approach and has a low computationally complexity. A 24×24 transmitarray generating a fan-beam near-field pattern has been synthesized in 340 seconds, demonstrating the effectiveness and efficiency of the procedure. The degradation of the near-field pattern and the amplitude loss due to a uniform quantization of the optimal phase profile have been evaluated. Results show that a phase quantization finer than 3 bits is required to approach the optimal results, though relatively good performance are obtained with a 2-bit quantization. These findings suggest that simple electronically reconfigurable transmitarrays may be used for dynamic near-field shaping.

Acknowledgements

This work was supported in part by MICIN/AEI/10.13039/501100011033 within the project PID2020-114172RB-C21; and by the Gobierno del Principado de Asturias under project AYUD/2021/51706.

References

[1] A. Razavi, R. Maaskant, J. Yang, and M. Viberg, “Optimal aperture Distribution for near-field detection of foreign objects in lossy media,” in *Proc. IEEE-APS Topical Conf. Antennas Propag. Wireless Comm.*, Palm Beach, Aruba, 2014, pp. 659–662.

[2] X. He, W. Geyi, and S. Wang, “Optimal design of focused arrays for microwave-induced hyperthermia,” *IET Microw., Antennas Propag.*, vol. 9, no. 14, pp. 1605–1611, 2015.

[3] A. Buffi, A. A. Serra, P. Nepa, H. T. Chou, and G. Manara, “A focused planar microstrip array for 2.4 GHz RFID readers,” *IEEE Trans. Antennas Propag.*, vol. 58, no. 5, pp. 1536–1544, Mar. 2010.

[4] I. Iliopoulos *et al*, "3-D Shaping of a Focused Aperture in the Near Field," *IEEE Trans. Antennas Propag.*, vol. 64, no. 12, pp. 5262-5271, Dec. 2016.

[5] D. R. Prado, J. A. López Fernández, M. Arrebola, M. R. Pino and G. Goussetis, "General Framework for the Efficient Optimization of Reflectarray Antennas for Contoured Beam Space Applications," *IEEE Access*, vol. 6, pp. 72295-72310, 2018.

[6] F. Foglia Manzillo, O. Koutsos, B. Fuchs, R. Sauleau and A. Clemente, "Synthesis and Characterization of a Focused-Beam Transmitarray Antenna at 300 GHz," *Eur. Conf. Antennas and Propag. (EuCAP)*, 2022.

[7] Á. F. Vaquero. “Development of techniques for the analysis and synthesis of spatially-fed arrays for emerging applications in near-field”, *Ph.D. dissertation,* Univ. Oviedo, Sept., 2021.

[8] S. Loredo, G. León and E. G. Plaza, "A Fast Approach to Near-Field Synthesis of Transmitarrays," *IEEE Antennas Wirel. Propag. Lett.*, vol. 20, no. 5, pp. 648-652, May 2021.

[9] G. -B. Wu, K. F. Chan and C. H. Chan, "3-D Printed Terahertz Lens to Generate Higher Order Bessel Beams Carrying OAM," *IEEE Trans. Antennas Propag.,* vol. 69, no. 6, pp. 3399-3408, June 2021.

[10] A. Clemente, F. Foglia Manzillo, M. Śmierzchalski and R. Sauleau, "Electronically-Steerable Transmitarray Antennas for SATCOM Terminals: a System Perspective," *(iWAT)*, 2020, pp. 1-4.

[11] F. Foglia Manzillo, M. Smierzchalski, J. Reverdy and A. Clemente, "A Ka-band Beam-Steering Transmitarray Achieving Dual-Circular Polarization," *15th Eur. Conf. Antennas Propag. (EuCAP),* 2021.

[12] Hansen, J. E. (ed.): ‘Spherical Near-field Antenna Measurements’ (Electromagnetic Waves, 1988)

[13] F. Foglia Manzillo *et al* "A highly directive D-Band antenna module comprising a flat discrete lens and an active feed," Proc. *IEEE Int. Symp. Antennas Propag. (AP-S/URSI)*, pp. 321-322, Denver, USA, July 2022.

[14] C. A. Balanis, Antenna Theory: Analysis and Design, 3rd Ed. Hoboken, NJ, USA: Wiley Interscience, 2005.